Torque and switching in the bacterial flagellar motor

An electrostatic model

Richard M. Berry
The Clarendon Laboratory, Oxford OX1 3PU, United Kingdom

ABSTRACT A model is presented for the rotary motor that drives bacterial flagella, using the electrochemical gradient of protons across the cytoplasmic membrane. The model unifies several concepts present in previous models. Torque is generated by proton-conducting particles around the perimeter of the rotor at the base of the flagellum. Protons in channels formed by these particles interact electrostatically with tilted lines of charges on the rotor, providing "loose coupling" between proton flux and rotation of the flagellum. Computer simulations of the model correctly predict the experimentally observed dynamic properties of the motor. Unlike previous models, the motor presented here may rotate either way for a given direction of the protonmotive force. The direction of rotation only depends on the level of occupancy of the proton channels. This suggests a novel and simple mechanism for the switching between clockwise and counterclockwise rotation that is the basis of bacterial chemotaxis.

1. INTRODUCTION

The bacterial flagellar motor is the device that couples transmembrane flux of ions to rotation of helical flagella in bacterial cell envelopes, providing a means of propulsion for the bacteria. The ion involved is usually H^+ but also can be Na^+ in alkalophilic bacteria that live in environments with very low H^+ concentrations (1, 2). The driving force for rotation is generated at the basal body that is embedded in the cell envelope and transmitted to the flagellum via the flexible "hook." Gram-positive bacteria have two discs, the M- and S-rings, which are coplanar with the inner plasma membrane and are both composed of the same protein (3). These discs form part of the rotor and are involved in the process of torque generation, either directly or as a mounting for active components of the motor. Gram-negative bacteria have a further two discs, the L- and P-rings, which act as bearings through the outer membrane and are not believed to play any role in force generation. The discs are ~300 Å in diameter and 50 Å thick, as inferred from image reconstruction of electron micrographs (4).

Complicated systems of chemotaxis allow bacteria to detect changes in their environment and seek out favorable growth conditions. Different bacteria achieve this in different ways, but in all cases stopping or reversal of the flagellar motor is involved (5). Switches between clockwise (CW) and counterclockwise (CCW) rotation in wild-type cells occur without changes in the direction of the transmembrane protonmotive force (pmf), indicating two separate modes of operation for the flagellar motor. Force generation is thought to occur at independent units embedded in the cytoplasmic membrane peripheral to the rotor and consisting of the proteins MotA and MotB. Freeze-fracture electron micrographs of bacterial cell envelopes show particle rings surrounding holes of ~300 Å. These rings consist of 10–12 particles in *Streptococcus* or 14–16 particles in *Escherichia coli* and are absent in certain nonmotile mutants. Simultaneous introduction of MotA and MotB leads to recovery of both motility and the ring structures (6). Furthermore, addition of both Mot proteins restores motor torque in discrete steps, providing evidence for eight independent force generators (7). Each generator is capable of rotating either CW or CCW with approximately equal torque in both directions. There is evidence that MotA is the proton-conducting component of the flagellar motor (8), whereas MotB is believed to anchor the force generators to the cell wall (7).

For motors driven by influx of protons, as in metabolizing bacteria, there are in fact three modes. In addition to CW and CCW rotation, there is a "pausing" state where the motor does not rotate (9). In enteric bacteria such as *E. coli,* the CCW rotating state is thought to be the "natural" state, in that mutants with chemotaxis genes *che*A–*che*Z deleted have CCW-only motors. The trigger for pausing and CW rotation appears to be the phosphorylated CheY protein (10, 11), which receives its phosphate group from the phosphokinase protein CheA under the control of the chemotaxis system (12).

1.1. Parameters of motor function

Of particular interest to the biophysicist are the dynamic properties of the motor–torque generation and energy transduction. Various experiments have measured motor torque and proton flux under various conditions. In "tethered cell" preparations, bacteria have their flagella bound to the microscope slide by antibodies, and the torque of the motor causes the whole cell body to rotate slowly (typically at <10 Hz). The motors of free-swimming cells, on the other hand, rotate at up to 300 Hz and are found to operate at lower torque than those in tethered cells. In both cases inertial forces are negligible compared with viscous drag (due to the small size of bacteria), and the rotation rate of the motor is proportional to the motor torque. A brief summary of the dynamic properties discovered to date is given below.

(*a*) The stall torque of the motor is approximately equal to the torque under the high-load conditions of tethered cells (13). This torque is proportional to protonmotive force, whether as a transmembrane voltage

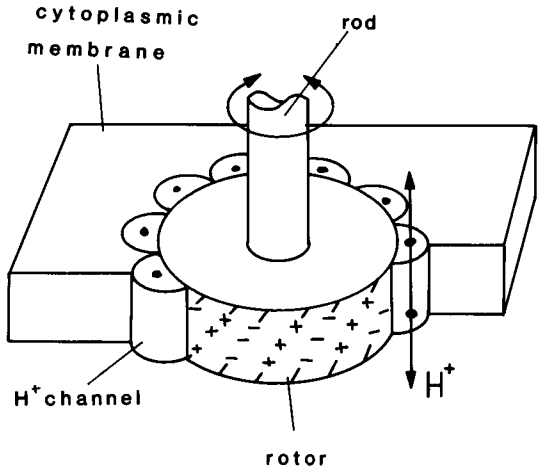

FIGURE 1 The rotor and torque-generating stator particles are flush with the inner membrane. The stator units are anchored to the cell wall by motB proteins (not shown) and contain H^+ channels. The rotor has alternating lines of positive and negative charges close to its perimeter. Torque is generated by electrostatic forces between these charges and protons passing through the channels. As a positively charged proton moves into the cell, it attracts negative charges on the rotor. Because the lines of charges are tilted with respect to the channels, this attraction causes the rotor to rotate CCW and generate CCW torque.

(V_m) or a pH gradient (ΔpH) (14). A typical value of stall torque would be ~700 kT or 25×10^{-12} dyn cm (15).

(*b*) Motor torque falls approximately linearly with increasing rotation rate (15).

(*c*) The rotation-dependent flux of protons corresponds to ~1,000 protons per revolution of the motor (to within a factor of two) (16). This is the change in flux on stopping the rotation of flagella and does not measure any flux through stalled motors. Motor efficiency calculated from this flux is near 100% at low rotation rates, falling to ≃5% under swimming conditions.

(*d*) Energized motors run smoothly (17) and respond quickly (response times of a few of milliseconds) to changes in pmf (18–20).

(*e*) Both tethered rotation rates and swimming speeds fall to zero at high and low values of pH (14). This occurs in CW-only *Streptococcus* mutants, indicating that it is an intrinsic feature of the force-generating system. The CW/CCW balance of nonmutant bacteria is also dependent on pH (21) and pmf (22).

2. A MODEL FOR THE FORCE GENERATOR OF THE FLAGELLAR MOTOR

Fig. 1 shows a simple model for the force-generating unit at the base of bacterial flagella. The rotor is connected to the flagellum via the rod and is free to rotate in the plane of the cytoplasmic membrane. Positive and negative charges are arranged around the perimeter of the ring such that they provide lines of alternating high and low electrical potential. These lines are oblique to the plane of the membrane as shown in the figure. The proton-conducting stator elements correspond to the particle rings seen in freeze-fracture electron micrographs (6) and are formed at least in part by the MotA protein.

The essential feature of the model is that the lines of charges on the rotor are tilted with respect to the proton channels in the stator elements. Protons flowing into the cell through the channel will exert a long-range electrostatic force on the charges on the rotor. As a proton moves through the channel, this force will tend to rotate the rotor CCW (as seen from outside the cell), keeping a line of negative charge adjacent to the positively charged proton. It may be useful to draw an analogy with a hydroelectric turbine: the water representing the protons and the turbine blades representing the charged lines on the rotor. Water flowing through the turbine exerts torque on the blades but need not necessarily cause the turbine to rotate if the resistance to rotation is high.

Fig. 2 shows electrostatic energies for the model motor in the two-dimensional space defined by the position of an ion in a channel (Z) and the rotation angle (x). Because of the tilt of the charged lines on the rotor, there are oblique valleys of low energy at positions where the proton in a channel is adjacent to a line of negative charges on the rotor. Proton influx is coupled to positive rotation as the system will tend to follow the valleys of low energy. Continuous, smooth passage of protons through the channels will cause continuous, smooth rotation of the rotor. This is similar to the model of Lauger (23), where protons flowing into the cell must always be at the intersection of two "half-channels" provided by the rotor and stator. In this model, however, protons are not artificially constrained by a tight-coupling condition as in Lauger's model but kept close to negative lines on the rotor by energetic considerations.

2.1. Computer simulation

For the sake of simplicity, the proton channel is initially represented by a chain of two discrete proton-accepting sites, one third and two thirds of the electrical distance across the channel. This simplification allows analytical solutions of the model in the limit of slow rotation rates and is useful to illustrate as clearly as possible the basic principles of the model, especially the proposed new switching mechanism. It does, in fact, also introduce an artificial constraint on the model, which is discussed along with its consequences in section 3.5.

Fig. 3, *a* and *b* shows the motor viewed in the plane of the membrane and from outside the cell. Each line on the rotor consists of two charges. There are n_r repeating units around the rotor so that each covers an angle $\phi = 2\pi/n_r$. In Fig. 3, $n_r = 8$. The tilt of the charge lines is expressed in terms of the pitch, α, such that the angle between the first and last charges in a line is given by $\alpha\phi$. It is useful to introduce the variable $x = n_r\theta$, where θ is the rotation angle of the rotor. One cycle of $x = 0 \rightarrow 2\pi$ then covers one repeating unit, ϕ, around the perimeter.

The kinetic diagram for a proton channel is shown in Fig. 3 *c*. State 1, or OO, is the empty channel. States 2

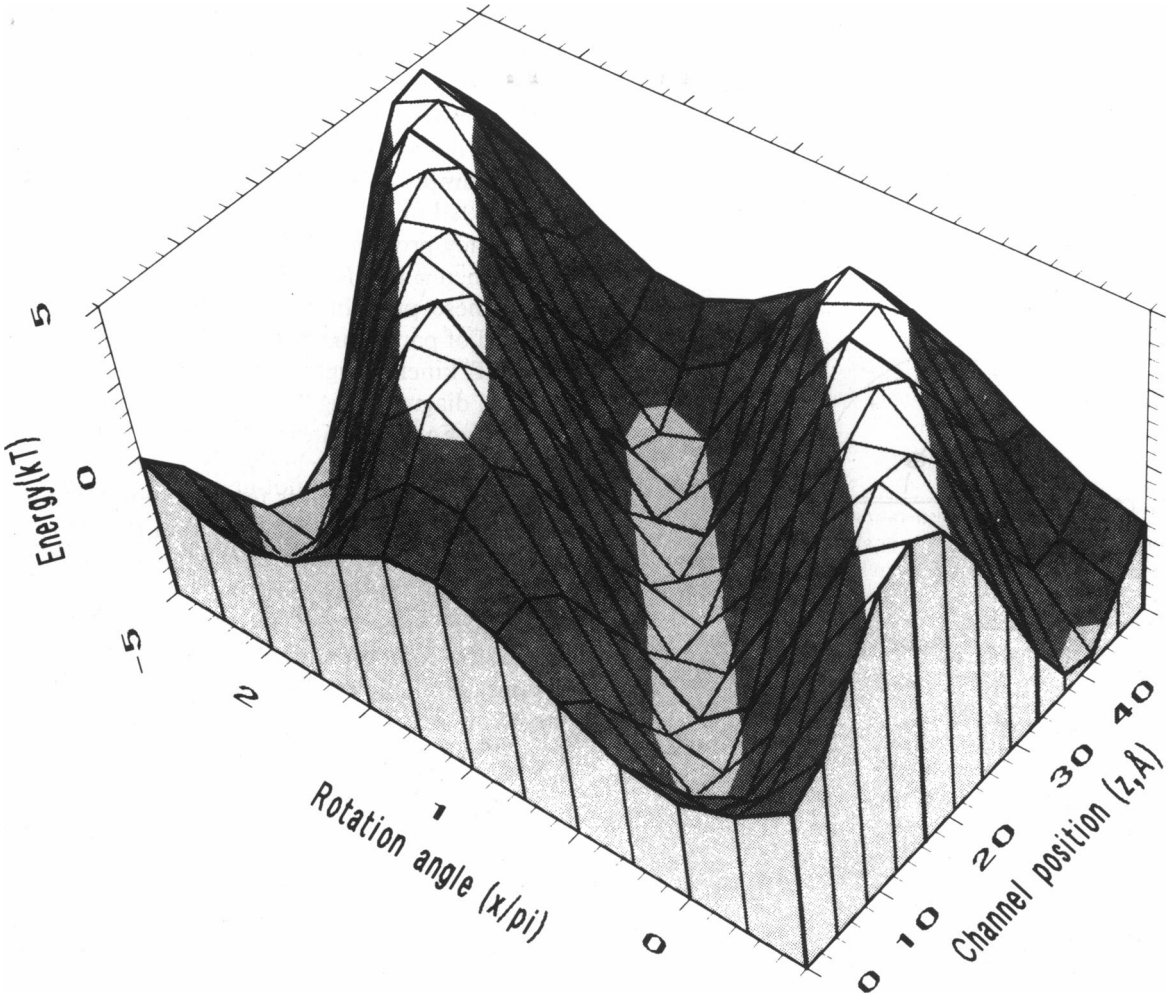

FIGURE 2 Electrostatic energies for the model motor in the two-dimensional space defined by the position of an ion in a channel (Z) and the rotation angle (x). Because of the tilt of the charged lines on the rotor, there are oblique valleys of low energy at positions where the proton in a channel is adjacent to a line of negative charges on the rotor. Proton influx is coupled to positive rotation because the system will tend to follow the valleys of low energy. These energies were calculated using the method of image charges for a membrane of thickness 50 Å and dielectric constant 2.5 in an aqueous medium of dielectric constant 80. The calculation uses six equally spaced univalent charges in each line on the rotor and a radial separation between these lines, and the channels of 10-Å contour levels are +4 kT and −4 kT.

(HO) and 4 (OH) are protonated at the external and internal sites, respectively. State 3, or HH, is the channel with both sites protonated. Protonated sites are positively charged, and empty sites are neutral. The energies of states 2–4 relative to the empty channel (state 1) are taken to be sinusoidal functions of rotation angle given by

$$U_2 = -A\cos(x) + U_k,$$
$$U_4 = -A\cos(x - \alpha) + U_k,$$
$$U_3 = U_2 + U_4 + US. \qquad (1)$$

A is the amplitude of the oscillations, α is the pitch of the lines of charge on the rotor, and US is the repulsion energy between the sites when both are protonated. Simple electrostatic energy calculations using the method of image charges (24) give energy functions U_i, which are indeed very nearly sinusoidal, and indicate that the values of amplitude (A) and repulsion (US) used in this work correspond to plausible arrangements of charges in the motor (Berry, R. M., unpublished results). U_k is the energy associated with the pK of the sites, given by

$$U_k = \ln(10^{7-pK}) \qquad (2)$$

such that U_k is defined as 0 at pK = 7.

The energies above are in fact the energies of the motor with protons at fixed positions one third and two thirds of the way across a channel, corresponding to discrete values of z in Fig. 2. Transitions between the states correspond to diffusion of protons through the smooth energy profile of the channel, $U(z)$, at any given rotation angle (x). Rate constants for such processes are in general complicated functions of the channel energy profile, and their detailed calculation is not trivial. One thing that is required, however, is that the ratio of forward and backward rates for a given transition must be $\exp(dU/$

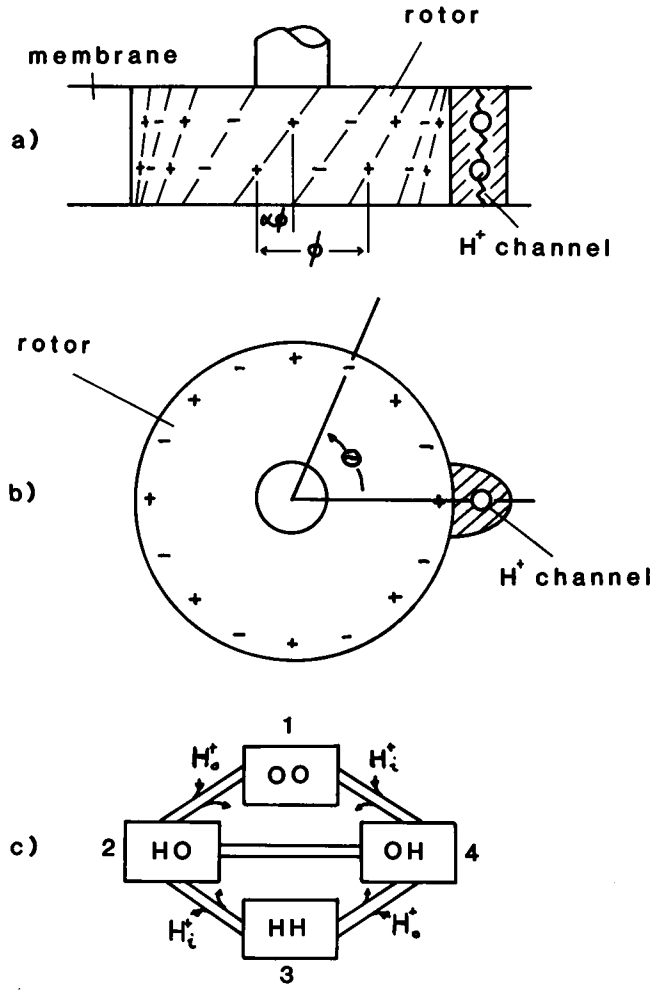

FIGURE 3 (*a*) The rotor and one channel protein (*shaded*), viewed in the plane of the membrane. The channel here is represented as a chain of two H^+-accepting sites, and there are two charges in each line on the rotor. The angle covered by one repeating unit on the rotor is ϕ, and $\alpha\phi$ is the angle between the first and last charges in a line. (*b*) The rotor and channel protein viewed from outside the cell. Only the outermost charge in each line is shown, and there are $n_r = 8$ repeating units or pairs of lines. The rotation angle, θ, is measured between the H^+ channel and the outermost charge on a negative line. (*c*) The kinetic diagram for a two-site, double-occupancy channel. State 1 (OO) is the empty channel, states 2 and 4 (HO, OH) are protonated at the external and internal sites, respectively, and state 3 (HH) is the doubly occupied channel. H_o^+ and H_i^+ represent uptake of protons from the external and internal solutions, respectively.

kT), where dU is the energy difference between the start and end points. This follows from statistical mechanics and is true for any transition at temperature T. We therefore calculate rate constants for transitions between states i and j as

$$k_{ij} = \exp((U_i - U_j)/2),$$
$$k_{ji} = \exp((U_j - U_i)/2). \quad (3)$$

This ensures the correct ratio and sets a basic transition rate of unity for all transitions between states of equal energy. In terms of Eyring theory, this is equivalent to assuming that all transition energy barriers are equal and that their peaks are situated halfway between the initial and final states.

If the motor runs smoothly at a constant rotation rate, ω, then rotation angles θ and x are proportional to time (the assumption of smooth running is discussed in section 3.5). For each position $x(t)$ we can calculate the occupancy probabilities $P_i(x)$ for each of the states i = 1–4. When ω is very small compared with all transition rates, these probabilities can be calculated using the method of partial diagrams (25). (We draw all possible "partial" kinetic diagrams that link all of the states in the original diagram [Fig. 3 *c* in this case] but that contain no loops. For each state (i), we then take the sum over all these partial diagrams (j) of terms like $k_{34}k_{42}k_{21}$, where the k's are rate constants for transitions leading toward the state (i) on the partial diagram (j). This sum over partial diagrams (Z_i) gives the relative probability of the state (i), and the state probabilities (P_i) are given by the normalized values of Z_i.) Such calculations correspond to the slow rotation rates observed in tethered cell preparations and shall be referred to as method one. When ω is larger, as in swimming cells, the probabilities are obtained by numerical integration. This method (method two) is used to investigate the dependence of motor function on rotation rate.

Torque is generated by electrostatic forces between protons in the channels and the charges on the rotor. The torque from each of the states 2–4 is proportional to the energy gradient ($-dU_i/d\theta$) and the occupancy probability ($P_i(\theta)$) of the state. Individual torques are then given by

$$T_i = -P_i(\theta)\frac{dU_i}{d\theta} = -P_i(x)\frac{dU_i}{dx}\cdot n_r. \quad (4)$$

The average torques are given by integrating over one cycle as

$$\langle T_i \rangle = 1/2\pi \int_0^{2\pi} T_i(x)\,dx, \quad (5)$$

and the total torque generated by one channel as

$$\langle T \rangle = \sum_i \langle T_i \rangle. \quad (6)$$

The total motor torque is then $\langle T \rangle \cdot n_c$, where n_c is the number of channels in the motor.

The instantaneous flux through each channel is equal to the flux over any one barrier, for example, the central barrier, and is given by

$$F(x) = P_2(x)k_{24} - P_4(x)k_{42}. \quad (7)$$

The average flux is

$$\langle F \rangle = 1/2\pi \int_0^{2\pi} F(x)\,dx, \quad (8)$$

and the total flux through the motor is $\langle F \rangle \cdot n_c$.

This is a loose coupled mechanism (26) in that proton flux and torque are connected only indirectly via the thermally activated proton occupancies of the channel sites. In tight coupled models, proton translocation is obligatorily coupled to rotation of the rotor.

3. RESULTS

3.1. Units and signs

Torque is given in units of (kT/channel $\div$ n_r), from $P_i(x)(dU_i/dx)$, and fluxes are in units of (ions/channel/time unit), where a time unit is the reciprocal of the basic transition rate set to unity in section 2.1. Flux and pmf are taken as positive when directed into the cell, and torque and rotation are positive when CCW as viewed from outside the cell. Rotation rates are in units of (cycles/time unit), $\omega = (1/2\pi)(dx/dt)$. For conversion to (revolutions/time unit) divided by n_r, the number of repeating cycles of positive and negative charge on the rotor.

3.2. The torque-generating cycle of the motor

Fig. 4 shows energies, occupancy probabilities, and torque for each of the channel states as functions of rotation angle during one cycle of the motor. The empty state OO has zero energy and generates no torque. The energies in Fig. 4 *a* are calculated from Eq. 1 with $A = US = 8$ kT ($\alpha = 0.25$ and p$K = 6.5$). The state occupancies in Fig. 4 *b* and torques in Fig. 4 *c* are calculated by method 1 (slow rotation) with external and internal pH 7 and a transmembrane voltage of 200 mV.

At $x = 0$ the external channel site is lined up with a negative charge on the rotor. A positively charged proton may enter from outside the cell and occupy the external site (moving the channel to state HO) but requires an extra 8 kT in energy to cross to the inner site (state OH). This makes proton transit with the rotor is locked at $x = 0$ unlikely. If, however, the rotor rotates to $x = 0.25\pi$, then the proton can pass to the inner site. The rotor may then continue to $x = \pi$, whereupon the proton can pass into the cytoplasm and return the channel to the empty OO state. This persists until the rotor rotates to $x = 1.5\pi$, where another proton may enter from outside the cell. The cycle couples the influx of a single proton to a rotation of $x = 2\pi$ or $1/n_r$ of a revolution of the rotor. The probability of the doubly occupied HH state is only 0.22% at p$K = 6.5$ due to the high repulsion energy between protonated sites ($US = 8$ kT), and the channel here is effectively single occupancy.

Torque generation may be understood as follows: protons occupying sites at angles where the energy gradient is negative exert positive torque on the rotor and, vice versa, the electrostatic forces tending to move the system toward energy minima. In the absence of a pmf, each state is occupied at angles where it has the lowest energy of the four, and the occupancy probabilities of adjacent

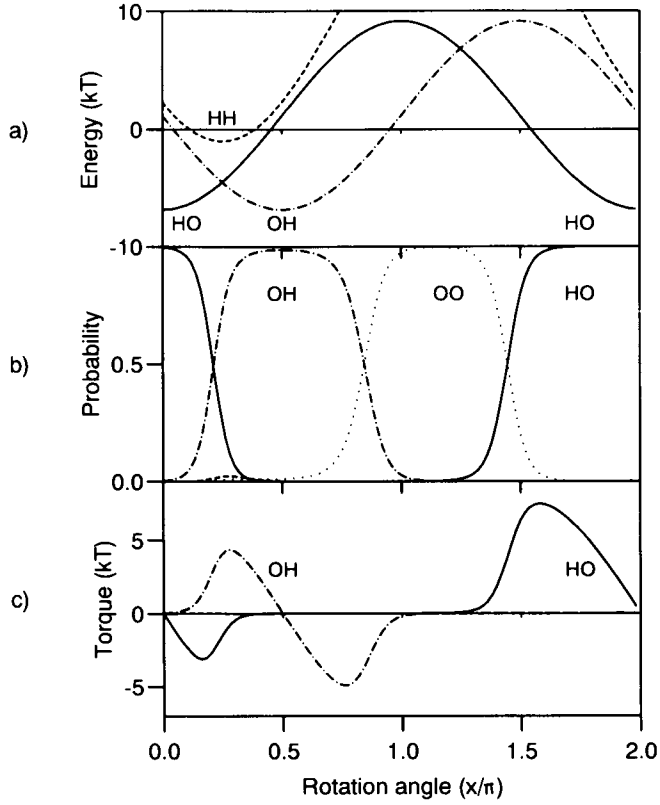

FIGURE 4 (*a*) Energies of the occupied states relative to the empty channel as functions of rotation angle for one cycle of the motor. The energies are given by Eq. 1 with $A = 8$ kT, $\alpha = 0.25$, $US = 8$ kT, and $U_k = 1.15$ kT (p$K = 6.5$). (*b*) Occupancy probabilities of the channel states, calculated by method 1 with a membrane voltage $V_m = 200$ mV. Because of the low pK and high site–site repulsion (US), the channel is often empty (OO) and hardly ever doubly occupied. Each state has a high probability of occupancy when it has the lowest energy of the four. The influx of ions due to the membrane voltage causes state 2 (HO) to be occupied preferentially at angles where its energy gradient is negative, generating a net positive torque. (*c*) The torque generated by each of the occupied states. Torque is the product of the energy gradient ($-dU/dx$) and the occupancy probability of the state.

states are equal at angles where the states have equal energy. With a pmf of 200 mV as in Fig. 4 *b*, however, the site occupancies are shifted toward lower angles. The state HO has an increased probability in its region of negative slope between $x = \pi$ and $x = 2\pi$ due to protons being driven into the external site by the pmf and a decreased probability between $x = 0$ and $x = \pi$ where protons can cross over to the internal site (state OH). Thus, the inward flux due to the pmf causes protons to occupy preferentially sites in the channel where they exert positive torque on the charges on the rotor. This torque causes the rotor to rotate such that the negative charges on the rotor remain close to protonated sites in the stator channel.

3.3. CW and CCW modes of rotation

Fig. 5 shows torque and state occupancies as functions of pK. Torques in Fig. 5 *a* are shown for amplitudes of 6, 8,

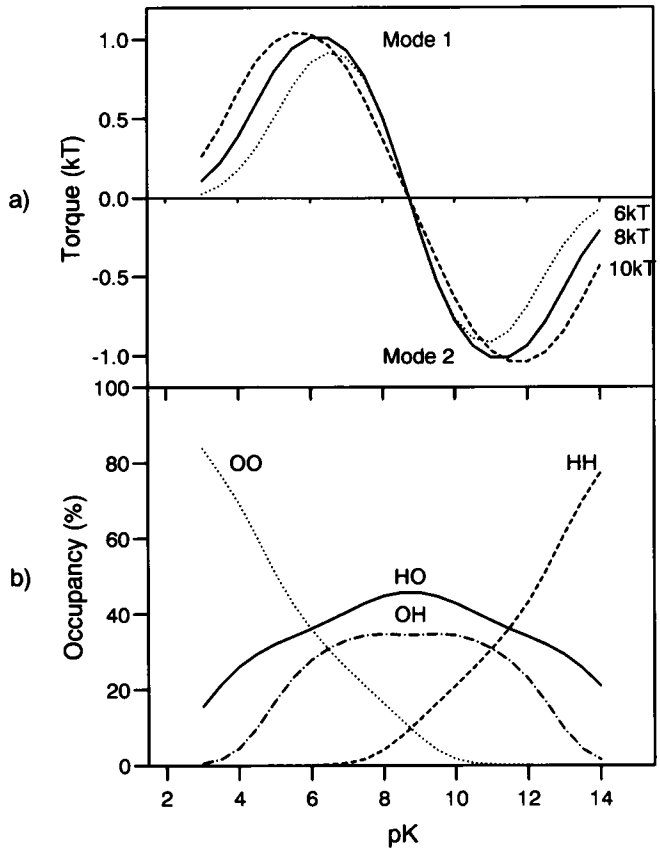

FIGURE 5 (*a*) Motor torque as a function of site pK for amplitudes A = 6, 8, and 10 kT. (*b*) Percentage occupancy probabilities for the four channel states at amplitude A = 8 kT. Depending on channel occupancy, the motor can generate either positive (mode 1) or negative (mode 2) torque for a given direction of proton flux. Parameters: α = 0.25; pH 7; US = 8 kT; V_m = 200 mV.

and 10 kT and occupancies in Fig. 5 *b* for A = 8 kT. Repulsion (US), pitch (α), pH, and transmembrane voltage are as in Fig. 4. Motor torque displays a positive peak at low pK and a negative trough of the same magnitude at high pK, with a zero torque point in between. The maximum positive torque for A = 8 kT occurs at pK = 6.5, the value used in Fig. 4, and the maximum negative torque is at pK = 11. The direction of rotation of the motor may be switched simply by changing the pK of the sites between these two values, whereas an intermediate pK gives a nonrotating or "pause" state. Low values of pK that generate positive torques and couple the influx of protons to CCW rotation shall be referred to as mode 1; high pK, negative torques, and CW rotation shall be referred to as mode 2.

In mode 2, at pK = 11, the probability of double occupancy (HH) is 30.7%, whereas the probability of the empty state (OO) is only 0.21%. In this case it is more useful to consider the "ground state" of the channel to be the doubly occupied HH state. The flux of protons into the cell is then realized by the flux of proton defects or "holes" out of the cell. Whereas before, in mode 1, protons followed the lines of negative charge on the rotor, now holes with a relative charge of −1 follow the positively charged lines. Since influx of protons is equivalent to efflux of holes and the pitch of the charged lines is the same, the rotor rotates in the opposite direction. Fig. 6 *a* shows the energies of the states OO, HO, and OH relative to the doubly occupied, doubly charged HH, Fig. 6 *b* shows the occupancy probabilities of the four states with pH 7 and a transmembrane voltage of 200 mV, and Fig. 6 *c* shows the torque generated by each state relative to the torque that would be generated at the same angle if the protons were in state HH. Fig. 6 bears a close resemblance to Fig. 4. The motor now rotates in the direction of decreasing x (as all torques are of the opposite sign) and the empty state is HH (no holes) rather than OO (no protons); otherwise the figures are very similar. This illustrates that holes and protons generate torque by the same mechanism but in opposite directions. The zero-torque point between modes 1 and 2 occurs when the probabilities of OO and HH are equal, and neither holes nor protons can be said to be the predominant charge carriers. This happens where $U_k = -US/2$ (at pK = 8.75 for US = 8 kT), and the repulsion energy is exactly com-

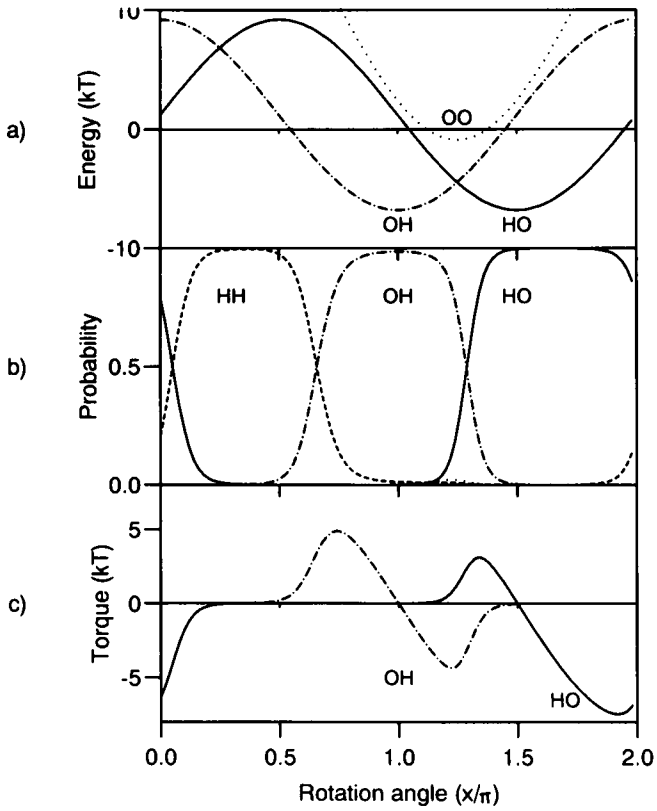

FIGURE 6 Energies, occupancy probabilities, and torques for each of the channel states as functions of rotation angle. Energies are given relative to the doubly occupied (HH) state and are thus the energies of proton defects or holes. Torques are proportional to the gradients of these energies and are thus hole torques. The membrane voltage is again 200 mV, and all parameters are the same as in Fig. 3 except that now pK = 11 (which gives U_k = −9.2 kT).

pensated by the intrinsic "pK" energy of protonating two sites.

The model assumes that protonated sites are positively charged, whereas deprotonated sites, or holes, are neutral. This is not important. The model would work equally well if the protonated sites were neutral and holes were negatively charged. In either case, the current carriers in the channel will attract lines of charge on the rotor, and the tilt of these lines will generate motor torque. When the current carriers are protons flowing into the cell, they will attract negatively charged lines and generate positive torque. When they are holes flowing out of the cell, they will attract positively charged lines and generate negative torque.

This section demonstrates that the model motor can be made to rotate in either direction for a given pmf. Switching between the modes is achieved by shifting the level of proton occupancy of the sites. We have shown this by varying site pK values, although changes in pH of the internal and external media would have the same effect. Changes of pK may be brought about simply by binding a charged ligand close to the H^+-channel sites (27). For instance, the negatively charged phosphate group on the phosphorylated CheY switching protein would attract positively charged protons into the channel if it bound nearby, increasing the pK of the channel sites. This provides a simple mechanism for the switching of the motor by phosphorylated CheY.

3.4. Dependence on pmf and rotation rate

Fig. 7 shows the dependence of torque on pmf for both modes of rotation (method 1). The amplitude (A) and repulsion (US) are both 8 kT, and the pitch (α) is 0.25. Mode 1, with positive or CCW torque, is at pK = 6.5, and mode 2 is at pK = 11. The inward directed pmf is present as a transmembrane voltage (V_m), high internal pH (ΔpH_a), or low external pH (ΔpH_b).

With the pmf as a voltage, V_m, torque is proportional to pmf for both modes. In addition, each mode generates torque of approximately the same magnitude, in accordance with experimental findings (28). The chemical potential ΔpH_a is equivalent to V_m, also as found experimentally (14), except for saturation at high values. With the pmf in the form of high hydrogen ion activity in the external medium (ΔpH_b), the mode 1 torque peaks and eventually falls below zero. This is because rising H^+ activity at low pH causes increased channel occupancy and results in mode 2 behavior. The torque becomes negative when the external pH is reduced below 4, corresponding to a pmf of 175 mV (internal pH = 7). This has the same effect on channel occupancy by protons from the external solution as increasing the pK by 3 units and keeping external pH 7. Such an increase would be enough to take the pK from 6.5 to 9.5 and into the mode 2 region of negative torque (see Fig. 5).

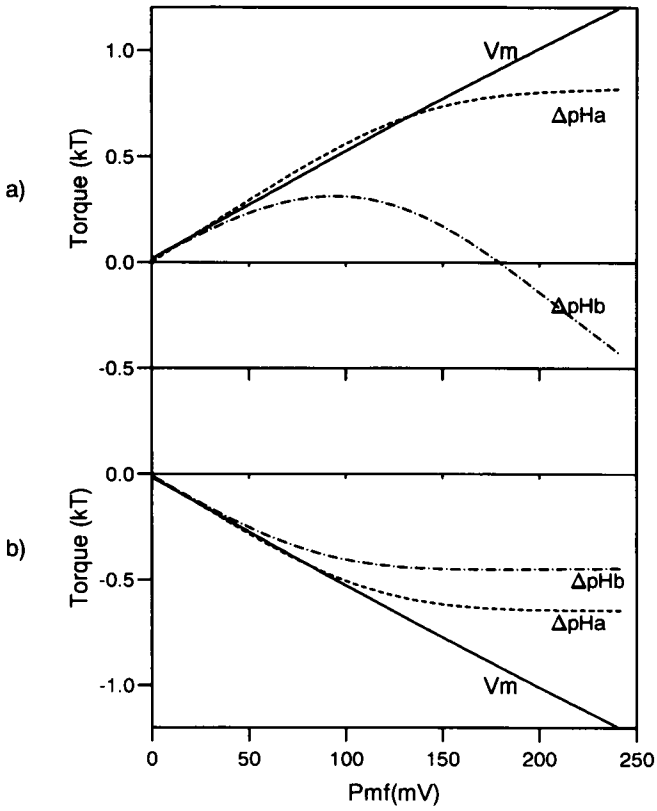

FIGURE 7 The dependence of torque on pmf. (a) Mode 1, pK = 6.5. (b) Mode 2, pK = 11. The pmf is present as a transmembrane voltage (V_m; $pH_i = pH_o = 7$), high internal pH (ΔpH_a; $pH_o = 7$, $pH_i > 7$) or low external pH (ΔpH_b; $pH_i = 7$, $pH_o < 7$) and is directed inward in all three cases. Parameters: A = 8 kT; pK = 6.5 (mode 1), 11 (mode 2); α = 0.25; US = 8 kT.

Fig. 8 shows flux and torque as functions of rotation rate with pmf of 0, 75, and 150 mV. These results are calculated using method 2 and with a purely electrical pmf. Solid lines are for mode 1 at pK = 6.5 and broken lines for mode 2 at pK = 11. Fig. 8 a shows that motor torque falls in approximately linear fashion with increasing ω, in keeping with experimental observations. Stall torque at 150 mV is +0.78 kT in mode 1 and −0.78 kT in mode 2. This compares with ~700 kT per motor as found in experiments with metabolizing *Streptococcus* cells (15) (where the pmf is ~150 mV [29]) and gives a value of $n_r n_c$ = 897 for the product of the number of channels and the periodicity of the charged lines on the rotor. If n_c = 8 (7), then this gives n_r = 112, whereas a value of 16 for n_c (30) would require n_r = 56. Fifty-six pairs of charge lines around a rotor of diameter 300 Å would correspond to a separation of 17 Å between each pair. The rotation rate for zero torque at 150 mV is ω_0 = 0.12. If this is to compare with the value ≃100 Hz found by Lowe et al. (15), then the unit transition rate in the model must be of order 10^4 s^{-1}, which is of the same order of magnitude as measured protonation and deprotonation rates in ion channels (31).

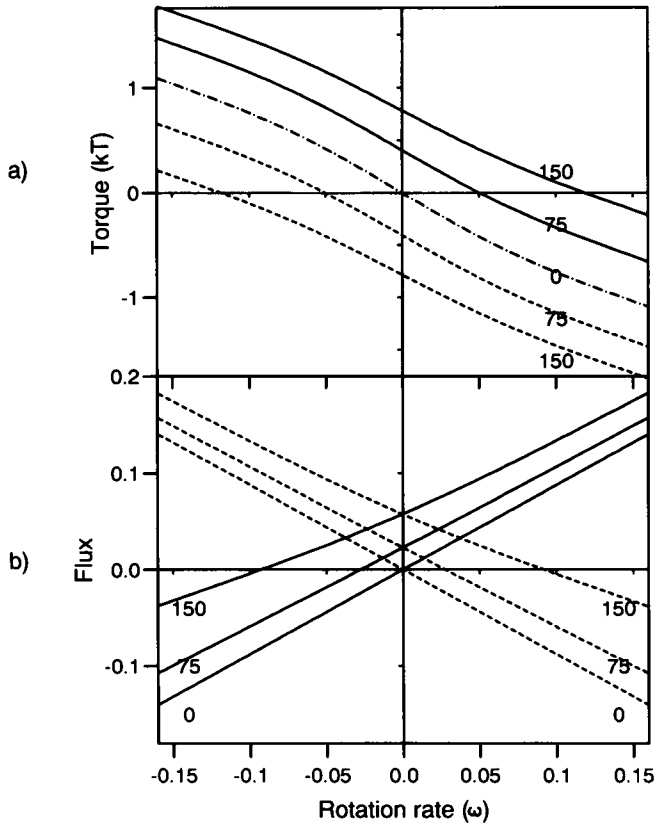

FIGURE 8 Motor torque and proton flux as functions of rotation rate for pmf of 0, 75, and 150 mV. Solid lines show results for mode 1 and broken lines for mode 2. (*a*) Motor torque increases in proportion to membrane voltage and decreases roughly in proportion to rotation rate. The motor torque in the absence of pmf is the same for both modes. (*b*) Ion fluxes show an approximately linear increase with rotation rate. This indicates a component of flux tightly coupled to rotation such that a fixed number of ions cross the membrane in one revolution of the motor. When the pmf is non-zero, there is also a rotation-independent or leakage flux, seen as a vertical offset in the curves. Influx of protons is coupled to positive torque and rotation in mode 1 and to negative torque and rotation in mode 2. Parameters: A = 8 kT; pK = 6.5 (mode 1), 11 (mode 2); pH 7; $\alpha = 0.25$; US = 8 kT; V_m = 0, 75, 150 mV.

The approximately linear dependence of flux on ω in Fig. 8 *b* indicates a component of flux tightly coupled to motor rotation. The slope corresponds to 0.87 ions per cycle per channel (for zero pmf where ion flux is entirely rotation dependent), indicating that the coupling is not quite perfect and that a cycle of the rotor may pass without the transit of a proton. With $n_r n_c = 897$, this rotation-dependent flux is equal to 780 ions per revolution per motor. Positive flux (protons into the cell) is coupled to CCW rotation ($\omega > 0$) in mode 1 and to CW rotation ($\omega < 0$) in mode 2.

The flux curves also have a vertical offset associated with rotation-independent or "leakage" current. This is a feature of the loose-coupled nature of the model and causes motor efficiency (equal to the output power ÷ the energy dissipated by proton flux) to tend toward zero at low rotation rates. Output power is the product of torque and ω and tends to zero as $\omega \rightarrow 0$, whereas the energy dissipated by the motor at low rotation rates is non-zero due to the leak current. The efficiency also falls at high ω as the torque and thus output power tends to zero. Peak efficiency is 27% at 75 mV and 23% at 150 mV. These efficiencies are calculated with the total proton flux, both rotation dependent and rotation independent, and cannot ever exceed 100%. Apparent efficiencies, calculated from rotation-dependent flux only, also fall as $\omega \rightarrow \omega_0$ but tend to values of 100% and more at low frequency. It is these apparent efficiencies that have been calculated in experiments (16) that disregard any leakage currents.

3.5. Effects of modeling channels as chains of discrete sites

We have modeled the proton channels in the motor as simple chains of two proton-accepting sites. This was done for the sake of simplicity and clarity, especially in the illustration of the possibility of mode 2 rotation. There are, however, some disadvantages to this assumption, which are discussed here along with their consequences for future developments of this model.

With only two sites to represent the channel, the association between each channel and a line of negative charges on the rotor are compromised. The progress from state HO to OH is really a continuous motion of the proton through the channel accompanied by a continuous increase of the rotation angle, taking the motor along one of the valleys of low energy in Fig. 2. With only two sites to represent the channel, however, this is replaced by a single large hop at a fixed angle. If the pitch of the charged lines (α) is >0.5, such a hop from HO to OH takes the proton nearer to the adjacent line of negative rotor charges than to the line on which it started. The resulting torque will pull this second line toward the channel, so that inward flux becomes coupled to negative rotation. In this case the valleys of low energy are not clearly defined by the two discrete values of channel position (z) chosen for the two sites. Because of this problem, a two-site representation of the model cannot have a pitch >0.5. This in turn means that there must be a large part of the motor cycle where there is no state capable of generating positive torque and where the channel will be empty (between $x = 0.5$ and $x = 1.5$ in Fig. 4). A single force-generating unit will therefore be unable to power the motor past this "dead zone," and the motor will be unable to run smoothly as assumed in the simulation. This is an artificial problem created by the reduction of the stator channels to chains of only two sites.

One solution would be to introduce a compensatory tight-coupling condition such that the transition between states HO and OH must be accompanied by a corresponding rotation of the rotor. This would make the model identical to that of Lauger (23) and lose the important feature of torque generation directly by electrostatic forces.

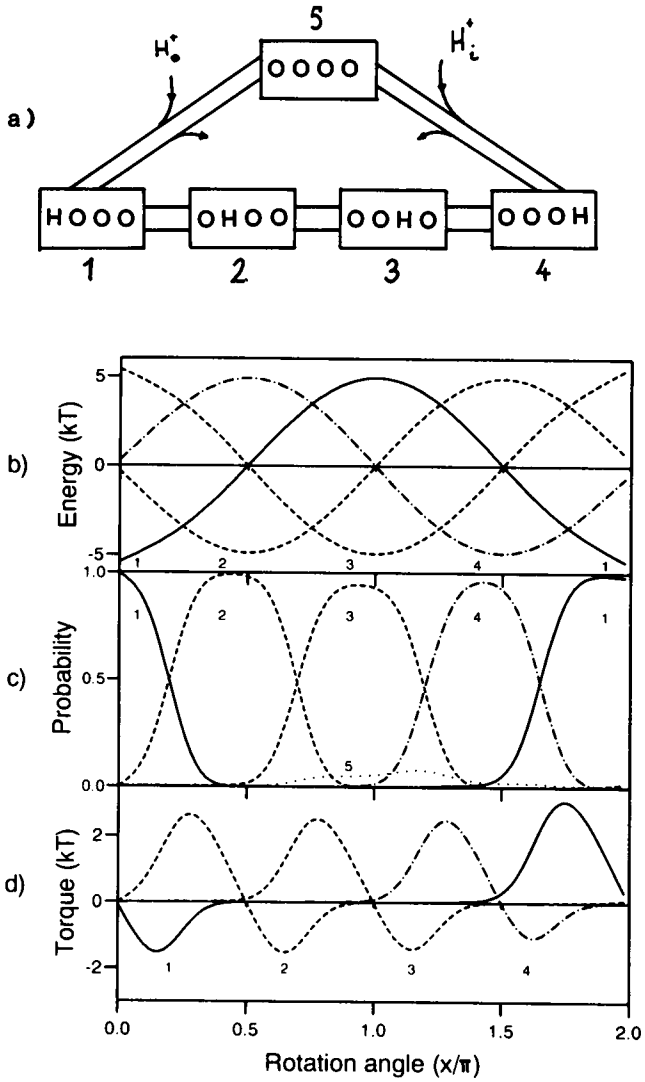

FIGURE 9 (*a*) The kinetic diagram for a four-site, single-occupancy channel. As in Fig. 3 *c*, H_o^+ and H_i^+ represent uptake of protons from the external and internal solutions, respectively. (*b*) Energies of the occupied states relative to the empty channel, as functions of rotation angle for one cycle of the motor. The energies are given by Eq. 9 with $A = 5$ kT, $\alpha = 0.75$, and $U_k = 0$ ($pK = 7$). (*c*) Occupancy probabilities of the channel states, calculated by method 1 with a membrane voltage $V_m = 150$ mV. As in Fig. 4, each state has a high probability of occupancy when it has the lowest energy of the five, and influx of ions due to the membrane voltage causes each state to be occupied preferentially at angles where its energy gradient is negative, generating a net positive torque. The mechanism is the same as that of Fig. 4 except that there are positive-torque–generating states at all angles, and the channel is hardly ever empty. (*d*) The average torque generated by each of the occupied states.

The simplest solution in the case of single-occupancy channels is to represent each channel by more than two states. The pitch is no longer restricted to values below 0.5, and inward movement of protons in a single channel can generate positive torque at any angle. Fig. 9 *a* shows the kinetic diagram for a four-site, single-occupancy channel. The energies in Fig. 9 *b* are those of the occupied states (1–4) relative to the empty channel and are given by

$$U_1 = -A\cos(x) + U_k,$$
$$U_2 = -A\cos(x - \alpha/3) + U_k,$$
$$U_3 = -A\cos(x - 2\alpha/3) + U_k,$$
$$U_4 = -A\cos(x - \alpha) + U_k, \qquad (9)$$

where $A = 5$ kT, $\alpha = 3/4$, and $U_k = 0$ ($pK = 7$).

Fig. 9 *c* shows occupancy probabilities of the five channel states, calculated by method 1 with a membrane voltage $V_m = 150$ mV. As in Fig. 4 *b*, each state has a high probability of occupancy when it has the lowest energy of the five. Influx of ions due to the pmf causes each state to be occupied preferentially at angles slightly below its energy minimum where its energy gradient is negative, and thus the torque is positive. The mechanism is the same as mode 1 of the two-site version (Fig. 4) except that now there are positive-torque–generating states at all angles, and the channel is hardly ever empty. The dependence of motor torque and flux on pmf and rotation rate is qualitatively identical to that of the two-site version in mode 1. The four-site version is more efficient (43% at 150 mV as opposed to 23%) and has tighter coupling between flux and rotation. The leakage flux through a stalled motor is reduced ~10-fold, and the rotation-dependent flux at zero pmf is increased from 0.87 to 0.97 ions per cycle. These results indicate a high degree of coupling despite the essentially loose-coupled nature of the model. Fig. 9 *d* shows torques generated by each state.

Fig. 10 *a* shows the same torques as Fig. 9 *d* along with the total torque generated by all four occupied states together. At first glance one might say that the motor would be unable to get past angles $x = 0$, 0.5π, π, and 1.5π, where the total torque appears to be negative. This is not the case. The torques shown in the figures are calculated as the products of the probabilities (P_i) and the energy gradients ($dU_i/d\theta$) of the individual states. They are not instantaneous values but ensemble averages over all possible states of the channel at each given angle. The actual motor torque at a given instant will be determined by the instantaneous position of the proton and may be positive at angles just above $x = 0$ (for instance) if the channel is in state 2 (for these angles). This state is not as likely as state 1, but nonetheless has a non-zero probability due to thermal excitation. The probability of state 2 is enhanced by the membrane voltage driving protons into the cell, which is why the motor generates a net positive torque. Fig. 10, *b* and *c* shows that increasing the number of sites used to model the channels gives increasingly smooth torque generation (on average) so that the assumption of a constant rotation rate is a reasonable one for continuous channels.

The above results were all calculated with the assumption that the channels may be occupied only by one pro-

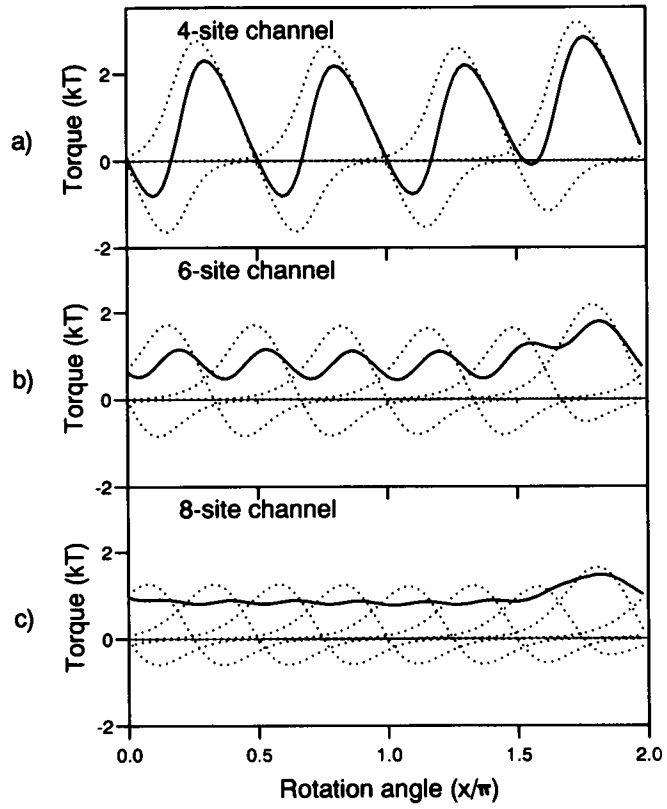

FIGURE 10 (*a*) The average torque generated by each of the occupied states (*dotted lines*) and the total average torque (*solid lines*) as functions of rotation angle for the four-site channel as in Fig. 9 *d*. Although there are angles where the total average torque is negative (near $x = 0$, 0.5π, π, and 1.5π), the motor can still generate positive instantaneous torque at these angles by the inward motion of a proton from the site with the highest occupancy probability at that angle. (*b*) Average torques as in *a* for a six-site channel and a membrane voltage $V_m = 150$ mV. Energy functions for the six occupied channel states are given by equations similar to Eq. 9, with $A = 5$ kT and $\alpha = 5/6$. The average total torque is positive at all angles in this case. (*c*) Average torques as in *a* and *b* for an eight-site channel. The pitch $\alpha = 7/8$ and $A = 5$ kT as before. As the number of sites used to model the channel increases toward the limit of a continuous channel, the average torque as a function of rotation angle becomes nearly constant. Such a motor would be expected to run smoothly. The total torque averaged over one whole cycle is similar in all three cases.

ton at a time. There are various possibilities for the physical form of channels with multiple-proton occupancy that could exhibit the occupancy-dependent switching mechanism presented in this work. It is unlikely that a channel in mode 2 will consist of a chain of many positively charged protonated basic sites and a single neutral hole. Aside from the high energy required to bring many positive charges into close proximity in the low dielectric constant of the membrane, there is the problem that the instantaneous motor torque will be dominated by the forces on these charges and that the effects of one site being neutral (the hole torque) will be insignificant. A more likely arrangement would be one where in mode 1 protons are conducted along chains of basic sites (positive charges moving into the cell), whereas in mode 2 holes or negative charges move out of the cell along chains of normally protonated acidic sites. Such a scheme would reverse the dependence of motor direction on site occupancy or pK, with high occupancy corresponding to protons on basic sites (mode 1) and low occupancy corresponding to holes on acidic sites (mode 2). The acidic and basic sites need not be separate. A channel consisting of a single chain of alternating acidic and basic sites could pass either positively charged protons or negatively charged holes, depending only on the level of proton occupancy.

4. DISCUSSION

4.1. Predictions of the model

Predictions of the model are listed below and compared, where possible, to experimental findings.

(*a*) Torque is proportional to pmf, and electrical and chemical (pH) gradients are equally effective at moderate values of pmf. This is in agreement with experiments on tethered cells (14).

(*b*) The dependence of torque on rotation rate is approximately linear, as found in experiments on swimming *Streptococcus* cells (15).

(*c*) The flux of protons coupled to rotation of the motor is constant at ~800 per revolution. This compares well with the very approximate values around 1,000 found by Meister et al. (16). The model also predicts a rotation-independent or leakage flux, a direct consequence of its loose-coupled nature. The maximum efficiency of the motor is ~25%, but apparent efficiencies calculated disregarding the leakage flux may be 100% or more at low rotation rates. At high ω the efficiency falls as the torque falls to zero at ω_0. These results are in agreement with the experimental findings of Meister et al. (16).

(*d*) The motor runs smoothly. Even with only one channel there will be $n_r = 50$–100 torque generating cycles per revolution, and the independent action of several force-generating units will further smooth rotation. Experimental findings (17) indicate that the motor does indeed run smoothly.

(*e*) The model predicts the two counter-rotating modes and the intermediate "pausing" state found in the motors of various bacteria (9). The rotating modes generate torque of approximately equal magnitude as found experimentally (28).

The trigger for switching from CCW to CW rotation is thought to be the phosphorylated form of the CheY protein (10, 12). The phosphate group on this molecule is likely to carry one or more negative charges at physiological pH (pK values for inorganic phosphate are 2.15 and 7.20 for the first and second ionizations, respectively). This negative charge could increase the occupancy probabilities of proton channels in the stator if CheY were bound nearby, thus causing the motor to switch. It is

perhaps more likely that the binding of phospho-CheY would affect site pK indirectly via conformational or electrical changes in and around the channel proteins. Cooperative effects here could then explain the rapid switching of rotational sense without detectable changes in speed, which indicates coupling between the switching of the separate force generators.

The model also predicts that the transition between modes 1 and 2 could be achieved if the channel occupancy were altered by varying pH. Reversal of the direction of rotation in nonswitching cells by changes in pH would support a switching mechanism of the type presented here, although care would need to be taken in interpreting such results due to the possible complication of pH tactic responses. The model is equally applicable to the Na^+-driven motors of alkalophilic bacteria: only the ion selectivity of the stator channels need to be changed. The proposed dependence of rotational direction on ion occupancy could perhaps better be tested by varying the concentration of Na^+ in experiments on tethered cells of nonswitching mutant strains of alkalophilic bacteria.

It also should be pointed out that this model can also accommodate more traditional switching mechanisms where a conformational transition alters the geometry of the motor. For example, a conformational change in the rotor that reversed the tilt of the charged lines would also reverse the direction of motor rotation.

(f) In this model, the flagellar motor generates force by long-range electrostatic interactions. We might therefore expect the sequence of the FliF protein of the M-ring (1) to be rich in charged residues, as is indeed the case (32). There is some evidence to suggest that the M-ring may serve simply as a mounting for the torque-generating switch complex (33). The amino acid sequence of the FliG switch complex protein is remarkable for clustering of its charged residues, with adjacent positive and negative residues particularly common (34). This makes it an ideal candidate for providing the alternating lines of positive and negative charges on the rotor that are central to the model presented here.

4.2. Comparison with previous models

Many diverse models have been proposed for the mechanism of the bacterial flagellar motor. Fuhr and Hagendorn (35) propose a model based on the phenomenon of electrorotation where torque is generated by oscillating electric fields tangential to the membrane, whereas Wagenknecht (36) suggests twisting conformations of the rod linked to proton binding. These models are atypical in that motor torque is not explicitly connected to proton flux through particles at the perimeter of the rotor.

Electrostatic models (37–40) are those where force generation is explicitly by coulomb interaction between hydrogen ions traversing the membrane and charges in the motor. A recurring theme (38–40) is a working cycle as follows. Protons are fed onto sites on the rotor from the external medium by a set of channels formed by one of the motor components. Electrostatic forces then pull them (and thus the rotor) around to a second type of channel that releases them into the cell cytoplasm. None of these electrostatic models predicts the full range of motor properties discussed here.

In the loose-coupled model of Oosawa and Hayashi (26, 41), flux and rotation are linked indirectly via thermally excited states of a proton-binding stator element. The model is essentially stochastic in nature as the energies involved in torque-generating steps are of the same order of magnitude as the thermal energy, kT. There is no one-to-one correspondence between proton flux and motor rotation: both rotation without flux (slippage) and flux without rotation (leakage) may occur depending on the conditions under which the motor is operating. The electrostatic models of Murata et al. (37) and Kobayasi (38) are also loose coupled.

In tight-coupled models, on the other hand, there is an arbitrary and obligatory correspondence between proton translocation and rotation. Mechanisms with such tight coupling (23, 42) are easy to imagine as macroscopic systems but may be less realistic on the microscopic scale of the bacterial flagellar motor. The distinction between loose- and tight-coupled models is not so much about the actual torque-generating mechanism as the nature of the assumptions made in order to perform mathematical simulations and obtain quantitative results. Tight-coupling constraints are simplifications introduced to assist mathematical treatment, and tight-coupled models have to include an elastic link between the proton-conducting stator elements and the cell wall to allow for the smooth running of flagellar motors. Without this feature, rotation of the rotor would require simultaneous proton transitions in all of the force-generating units, a process with an intrinsically low probability. The model of Kleutsch and Lauger (43) permits rotation and flux to occur independently of each other, thus mimicking a loose-coupled mechanism. Slippage is allowed where the rotor rotates but the proton channels are not occupied, whereas leakage is a consequence of futile force-generating cycles extending the elastic linkage but not sufficiently to move the rotor.

The current model incorporates elements of all three categories above. Structurally, it resembles the model of Lauger (23), where protons are conducted at the intersection of "half-channels" on the rotor and stator and torque generation is a consequence of the relative slant of these half-channels. On the other hand, the model is loose coupled, and the method of calculating torques is similar to that of Oosawa and Hayashi. (The rotation rate is assumed, and corresponding values of torque and flux follow from the occupancy probabilities of the channel states. In tight-coupled models the starting point is the motor torque, which affects the rate constants of proton transitions. These give the flux directly, and the rotation rate follows from the assumptions of tight coupling

and elastic linkage to the cell wall.) Furthermore, torque generation is explicitly electrostatic, and the energy functions for the channel states may be calculated from a specific arrangement of charges corresponding to actual motor elements.

The predicted results of the model are very similar to those of both Kleutsch and Lauger and Oosawa and Hayashi. The existence of two counter-rotating modes, however, is a new feature. Previous models assume switching to occur as the result of major conformational changes that alter the arrangement of the motor components. The present model can generate CW, CCW, or no torque, depending only on the level of occupancy of the channel sites. This lends itself to a simple, electrostatic mechanism for switching of the motor by the phosphorylated CheY protein.

I am grateful to the Science and Engineering Research Council for the award of a graduate studentship, to my supervisor Dr. Donald Edmonds for support and encouragement, and to Dr. Judith Armitage for valuable advice on things bacteriological.

Received for publication 12 August 1992 and in final form 9 October 1992.

REFERENCES

1. Jones, C. J., and S. I. Aizawa. 1991. The bacterial flagellum and flagellar motor—structure, assembly and function. *Adv. Microb. Physiol.* 32:109–172.
2. Hirota, N., and Y. Imae. 1983. Na^+-driven motors of an alkalophilic bacillus strain Yn-1. *J. Biol. Chem.* 258:10577–10581.
3. Ueno, T., K. Oosawa, and S.-I. Aizawa. 1992. The m-ring, s-ring and proximal rod of the flagellar basal body of *Salmonella typhimurium* are composed of subunits of a single protein, FliF. *J. Mol. Biol.* 227:672–677.
4. Stallmeyer, M. J. B., S-I. Aizawa, R. M. Macnab, and D. J. DeRosier. 1989. Image reconstruction of the flagellar basal body of *Salmonella typhimurium*. *J. Mol. Biol.* 205:519–528.
5. Manson, M. D. 1992. Bacterial motility and chemotaxis. *Adv. Microb. Physiol.* 33:277–346.
6. Khan, S., T. S. Reese, and M. Dapice. 1988. Effects of Mot gene expression on the structure of the flagellar motor. *J. Mol. Biol.* 202:575–584.
7. Blair, D. F., and H. C. Berg. 1988. Restoration of torque in defective flagellar motors. *Science* (Wash. DC). 242:1678–1681.
8. Blair, D. F., and H. C. Berg. 1990. The mot A protein of *Escherichia coli* is a proton-conducting component of the flagellar motor. *Cell.* 60:439–449.
9. Eisenbach, M., A. Wolf, M. Welch, S. R. Caplan, I. R. Lapidus, R. M. Macnab, H. Aloni, and O. Asher. 1990. Pausing, switching and speed fluctuation of the bacterial flagellar motor and their relation to motility and chemotaxis. *J. Mol. Biol.* 211:551–563.
10. Barak, R., and M. Eisenbach. 1992. Correlation between phosphorylation of the chemotaxis protein CheY and its activity at the flagellar motor. *Biochemistry.* 32:1821–1826.
11. Kuo, S. C., and D. E. Koshland. 1989. Multiple kinetic states for the flagellar motor switch. *J. Bacteriol.* 171:6279–6287.
12. Hess, J. F., K. Oosawa, N. Kaplan, and M. I. Simon. 1988. Phosphorylation of three proteins in the signalling pathway of bacterial chemotaxis. *Cell.* 53:79–87.
13. Meister, M., and H. C. Berg. 1987. The stall torque of the bacterial flagellar motor. *Biophys. J.* 52:413–419.
14. Khan, S., M. Dapice, and I. Humayun. 1990. Energy transduction in the bacterial flagellar motor—effects of load and pH. *Biophys. J.* 57:779–796.
15. Lowe, G., H. C. Berg, and M. Meister. 1987. Rapid rotation of flagellar bundles in swimming bacteria. *Nature (Lond.).* 325:637–640.
16. Meister, M., H. C. Berg, and G. Lowe. 1987. The proton flux through the bacterial flagellar motor. *Cell.* 49:643–650.
17. Khan, S., M. Meister, and H. C. Berg. 1985. Constraints on flagellar rotation. *J. Mol. Biol.* 184:645–656.
18. Shimada, K., and H. C. Berg. 1987. Response of the flagellar rotary motor to abrupt changes in extracellular pH. *J. Mol. Biol.* 193:585–589.
19. Kudo, S., Y. Magariyama, and S.-I. Aizawa. 1990. Abrupt changes in flagellar rotation observed by laser dark-field microscopy. *Nature (Lond.).* 346:677–680.
20. Kami-ike, N., S. Kudo, and H. Hotuni. 1991. Rapid changes in flagellar rotation induced by external electric pulses. *Biophys. J.* 60:1350–1355.
21. Ravid, S., M. Eisenbach, and P. Matsumura. 1986. Restoration of flagellar clockwise rotation in bacterial envelopes by insertion of the chemotaxis protein cheY. *Proc. Natl. Acad. Sci. USA.* 83:7157–7161.
22. Khan, S., and R. M. Macnab. 1980. Proton chemical potential, proton electrical potential and bacterial energy. *J. Mol. Biol.* 138:599–614.
23. Lauger, P. 1988. Torque and rotation rate of the bacterial flagellar motor. *Biophys. J.* 53:53–65.
24. Neumcke, B., and P. Lauger. 1969. Nonlinear electrical effects in lipid bilayer membranes. *Biophys. J.* 9:1160–1170.
25. Hill, T. L. 1966. Studies in irreversible thermodynamics. IV. Diagrammatic representation of steady state fluxes for unimolecular systems. *J. Theor. Biol.* 10:442–459.
26. Oosawa, F., and S. Hayashi. 1986. The loose-coupling mechanism in molecular machines. *Adv. Biophys.* 22:151–183.
27. Edmonds, D. T. 1989. A kinetic role for ionizable sites in membrane channel proteins. *Eur. Biophys. J.* 17:113–119.
28. Berg, H. C. 1974. Dynamic properties of bacterial flagellar motors. *Nature (Lond.).* 249:77–79.
29. Kashket, E. R. 1985. The proton motive force in bacteria: a critical assessment of methods. *Annu. Rev. Microbiol.* 39:219–242.
30. Block, S. M., and H. C. Berg. 1984. Successive incorporation of force-generating units in the bacterial rotary motor. *Nature (Lond.).* 309:470–472.
31. Prod'hom, B., D. Pietrobon, and P. Hess. 1987. Direct measurement of proton transfer rates to a group controlling the dihydropyridin-sensitive Ca^+ channel. *Nature (Lond.).* 329:243–246.
32. Jones, C. J., M. Homma, and R. M. Macnab. 1989. L-, P-, and M-ring proteins of the flagellar basal body of *Salmonella typhimurium:* gene sequences and deduced protein sequences. *J. Bacteriol.* 171:3890–3900.
33. Yamaguchi, S., S.-I. Aizawa, M. Kihara, M. Isomura, C. J. Jones, and R. M. Macnab. 1986. Genetic evidence for a switching and

energy-transducing complex in the flagellar motor of *Salmonella typhimurium*. *J. Bacteriol.* 168:1172–1179.

34. Kihara, M., M. Homma, K. Kutsukake, and R. M. Macnab. 1989. Flagellar switch of *Salmonella typhimurium:* gene sequences and deduced protein sequences. *J. Bacteriol.* 171:3247–3257.
35. Fuhr, G., and R. Hagedorn. 1989. Dielectric motors—a new hypothesis for the bacterial flagella. *J. Theor. Biol.* 139:39–59.
36. Wagenknecht, T. 1986. A plausible mechanism for flagellar rotation in bacteria. *FEBS (Fed. Eur. Biochem. Soc.) Lett.* 196:193–197.
37. Murata, T., H. Shimizu, and M. Yano. 1989. A model for bacterial flagellar motor—free-energy transduction and self-organization of rotational motion. *J. Theor. Biol.* 139:531–559.
38. Kobayasi, S. 1988. Diffusion motor as a model of flagellar motor of bacteria. *Ferro-electrics.* 86:335–346.
39. Mitchell, P. 1984. Bacterial flagellar motors and osmoelectric molecular rotation by an axially transmembrane well and turnstile mechanism. *FEBS (Fed. Eur. Biochem. Soc.) Lett.* 176:287–294.
40. Glagolev, A. N., and V. P. Skulachev. 1978. The proton pump is a molecular engine of motile bacteria. *Nature (Lond.).* 272:280–282.
41. Oosawa, F., and S. Hayashi. 1983. Coupling between flagellar motor rotation and proton flux in bacteria. *J. Physiol. Soc. Jpn.* 52:4019–4028.
42. Meister, M., S. R. Caplan, and H. C. Berg. 1989. Dynamics of a tightly coupled mechanism for flagellar rotation—bacterial motility, chemiosmotic coupling, protonmotive force. *Biophys. J.* 55:905–914.
43. Kleutsch, B., and P. Lauger. 1990. Coupling of proton flow and rotation in the bacterial flagellar motor—stochastic simulation of a microscopic model. *Eur. Biophys. J.* 18:175–191.